



ELSEVIER

Available online at www.sciencedirect.com

SCIENCE @ DIRECT®

Physica B ■ (■■■■) ■■■–■■■

PHYSICA B

www.elsevier.com/locate/physb

A long wavelength neutron monochromator for superthermal production of ultracold neutrons

C.E.H. Mattoni^a, C.P. Adams^b, K.J. Alvine^a, J.M. Doyle^a, S.N. Dzhosyuk^a,
R. Golub^c, E. Korobkina^c, D.N. McKinsey^{a,1}, A.K. Thompson^b, L. Yang^a,
H. Zabel^d, P.R. Huffman^{a,b,*}

^aHarvard University, Cambridge, MA 02138, USA

^bPhysics Department, National Institute of Standards and Technology, 100 Bureau Drive MS 8461, Gaithersburg, MD 20899, USA

^cHahn-Meitner-Institut, Berlin, Germany

^dRuhr Universitat Bochum, Bochum, Germany

Received 9 April 2003; received in revised form 9 April 2003; accepted 8 October 2003

Abstract

Production of ultracold neutrons (UCN) by single-phonon downscattering of cold neutrons from superfluid helium (the “superthermal process”) utilizes input neutrons only in a narrow wavelength band around 0.89 nm. Delivering a monochromatic 0.89 nm neutron beam to a superfluid helium target reduces backgrounds in the UCN production region with minimal loss in the UCN production rate. The design, construction, and testing of a 0.89 nm neutron monochromator is reported herein. This monochromator is constructed from nine tiled pieces of stage 2 potassium-intercalated graphite with mosaics between 1.1° and 2.1° and reflectivities of (73–91)% at 0.89 nm. In addition to stage 2 potassium-intercalated graphite, fluorophlogopite and stage 1 potassium-intercalated graphite are also characterized. © 2003 Published by Elsevier B.V.

PACS: 61.12; 71.20.T; 03.75.B; 28.20

Keywords: Neutron monochromators; Intercalated graphite; Fluorophlogopite; Mosaic crystal; Superthermal process; Ultracold neutron production

1. Introduction

Several technologies allow neutron wavelength selection. Mechanical velocity selectors can be

used to pass a narrow band of neutron velocities (and, therefore, wavelengths) while capturing the rest in a spinning helical neutron absorber [1,2]. Polycrystalline materials with Bragg edges can be used as a long-pass wavelength filter; the short wavelength neutrons are scattered out of the beam in a spacially broad pattern which can then be absorbed [3,4]. Thin-film multilayer and crystal monochromators, in contrast, diffract neutrons in a specific wavelength band away from the primary beam. A high-reflectivity monochromator is parti-

*Corresponding author. Physics Department, National Institute of Standards and Technology, 100 Bureau Drive MS 8461, Gaithersburg, MD 20899, USA. Tel.: +3019746465; fax: +3019261604.

E-mail address: paul.huffman@nist.gov (P.R. Huffman).

¹Present address: Princeton University, Princeton, NJ 08544, USA.

cularly useful, because it minimally affects the primary beam, except in the narrow wavelength band of diffracted neutrons. Thus, two potentially useful beams are created from one. In addition, certain applications find the monochromaticity of the diffracted beam a great advantage.

Our work on monochromators was motivated by the desire to produce a narrow-band 0.89 nm wavelength neutron beam specifically for use in producing ultracold neutrons (UCN) via superthermal downscattering [5,6]. UCN are neutrons with energy below $\sim 10^{-7}$ eV, low enough to be totally reflected from many materials. UCN have application for fundamental physics measurements as well as materials studies [7–9], but their use is limited by available fluxes. The “superthermal process”, in which a high density of UCN is built up through inelastic scattering of cold neutrons from a bath of superfluid ^4He , offers the possibility of achieving much greater UCN densities than sources in thermal equilibrium [10,11].

The superthermal process relies primarily on input neutrons in a narrow momentum band. The dispersion curves of the free neutron and the fundamental excitations of superfluid ^4He cross only at zero and at a momentum, $\hbar k^*$, corresponding to a neutron wavelength of 0.89 nm. To satisfy the momentum conservation law, UCN up to a momentum $\hbar k_{\text{UCN}}$ can be produced by single-phonon downscattering of cold neutron with momentum $\hbar k_{\text{cold}}$ in the band $|\hbar k_{\text{cold}} - \hbar k^*| \leq \hbar k_{\text{UCN}}$. This corresponds to neutron wavelength of (0.89 ± 0.01) nm [12,13]. While only a very small fraction ($< 1\%$) of the spectrum of a typical polychromatic cold neutron beam is within this production band, all of the non-0.89 nm neutrons contribute to materials activation of the UCN source. For experiments that are closely coupled to the superthermal UCN source, such as the measurement of the neutron lifetime using magnetically trapped UCN [5,6], or the proposed search for a neutron electric dipole moment [14], neutron-induced backgrounds are a serious issue. Although, depending on the neutron source spectrum, as much as 50% of the UCN production in the helium may be due to multiphonon scattering of non-0.89 nm neutrons [15], a significant increase in signal to background ratio can

result from filtering the wavelengths of input cold neutrons to only those in the 0.89 nm band.

Although monochromators are commonly employed at shorter wavelengths, working devices at 0.89 nm have been quite rare. Herein we describe the development of a high-reflectivity and low-absorption 0.89 nm neutron monochromator for use in an experiment to measure the lifetime of the free neutron [5,6]. Construction and characterization of the monochromator are discussed in detail.

2. Monochromator design

2.1. Constraints

The basic operation of monochromators can be well understood from simple diffraction principles. The Bragg condition defines the grazing angle θ_{B} at which incident neutrons of wavelength λ will diffract from a crystal with lattice spacing d as $n\lambda = 2d \sin \theta_{\text{B}}$, where n , called the order of diffraction, is any positive integer. For perfect single crystals, the line width for diffraction is extremely narrow, $\Delta\lambda/\lambda \sim 10^{-5}$ [16].

In most monochromator applications, the desired output wavelength spectrum is broad enough that an alternative to a perfect crystal, a “mosaic crystal” must be used [17,18]. Such a crystal is composed of many microscopic perfect crystals, each with an orientation that varies slightly from the crystal’s average overall orientation. The distribution of mosaic block orientations can, for most crystals, be described by a cylindrically symmetric Gaussian distribution function

$$W(\Delta) = \frac{1}{\sqrt{2\pi}\eta} e^{-\Delta^2/2\eta^2},$$

where Δ is the angular deviation of the mosaic block normal vector from the mean and η is the width of the distribution.

The design of our monochromator is constrained, in part, by the experimental setup we use at the National Institute of Standards and Technology (NIST) Center for Neutron Research (NCNR) NG-6 beamline. This is where the UCN trapping experiment is performed [6]. In order to efficiently transport the diffracted 0.89 nm neutron

beam to the trapping apparatus, the neutron monochromator must satisfy certain constraints on its d -spacing and mosaic. Specifically, to prevent blocking access to other beamlines, the Bragg angle θ_B should be in the range of 25–65°, therefore restricting the ratio of d/n to the range 0.49–1.05 nm. In addition, the mosaic is constrained by the divergence of the NG-6 beam which affects the number of UCN produced in the trapping apparatus. The divergence of 0.89 nm neutrons in NG-6 beam is $\pm 1^\circ$ (set by the critical angle of the ^{58}Ni guide). In order to efficiently diffract all of these neutrons, the monochromator should have a mosaic $\gtrsim 1^\circ$. On the other hand, as the mosaic angle is increased, the divergence of the diffracted beam increases. Since the trapping region must be positioned (for instrumental reasons) at least 1.5 m downstream of the monochromator, divergence of the beam plays a role in determining the total UCN production. Numerical simulations indicate that the optimal monochromator mosaic is about 1° . Increasing the mosaic from 1° to 2° reduces the number of trapped neutrons by approximately 15%. As will be discussed, the mosaics of the crystals used in the final monochromator assembly fall in the 1–2° range.

2.2. Long wavelength monochromator materials

Two materials for possible use as a long wavelength neutron monochromator are examined: mica and intercalated graphite. We are not aware of any other class of materials with a suitable d -spacing and mosaic that are easily obtained or fabricated.

2.2.1. Mica

Numerous types of mica crystals have in the past been considered and used as long-wavelength neutron reflectors. Micas are crystals in which a central alkali (typically potassium) atom separates two layers of aluminosilicate compounds [19]. Depending on the type of mica, the exact nature and structure of the aluminosilicate components may vary. The naturally occurring muscovite mica ($\text{KA}_3\text{Si}_3\text{O}_{12}\text{H}_2$) was used for long-wavelength neutron studies in the late 1950s [20]. Following

the development of techniques for growing synthetic micas, the perfluorinated mica, fluorophlogopite ($\text{KMg}_3(\text{Si}_3\text{Al})\text{O}_{10}\text{F}_2$), also became a possibility. Fluorophlogopite, known industrially as Thermica,² has a larger structure factor, and hence higher reflectivity, than the naturally occurring micas muscovite or phlogopite, due to the substitution of Mg for Al in some of the crystal sites, and the substitution of fluorine for hydroxide [19].

Goland and colleagues measured the lattice spacing of fluorophlogopite to be $d = 0.9963$ nm and first proposed its use as a monochromator in 1959 [20]. Later, a prototype UCN source was built based upon Doppler-shifted Bragg scattering from a rotating fluorophlogopite crystal [21–23]. Additional studies of mica reflectivity were performed as part of the construction of a second generation rotor at Los Alamos [19]. Other studies of fluorophlogopite neutron scattering properties have also been performed [24,25] and neutron scattering instruments using mica neutron optical elements have been built [26]. Many studies have noted the very narrow ($\approx 0.3^\circ$) intrinsic mosaic of mica [19,20,24]. Increasing the effective mosaic of mica by producing a fan of many thin mica layers was tested by several authors [21,24].

2.2.2. Graphite intercalation compounds

Graphite intercalation compounds (GICs) form a large class of materials in which atoms or molecules are inserted (intercalated) between the layers of hexagonal graphite. Graphite intercalation was first reported by Shafthäutl in 1841 [27]. Studies of the structure, dynamics, electronic properties, and transport properties have been widely pursued (see, for example, Refs. [28,29]).

Various GICs have been studied for possible use as long-wavelength monochromators. A group at the Institute Laue-Langevin (ILL) studied stage 1 compounds of potassium-, rubidium-, and cesium-intercalated graphite [30]. Based upon that work, a

²Certain trade names and company products are mentioned in the text or identified in illustrations in order to adequately specify the experimental procedure and equipment used. In no case does such identification imply recommendation of endorsement by the NIST, nor does it imply that the products are necessarily the best available for the purpose.

stage 1 potassium-intercalated graphite monochromator was built and used for 0.756 nm neutron monochromatization on the DB21 low-resolution biological diffractometer at the ILL [31]. Alkali-intercalated graphites have the advantage of large structure factors, and hence high expected reflectivity for long-wavelength neutrons. Their disadvantage is that due to the high reactivity of the alkali metals, alkali intercalation compounds must never be exposed to oxygen or water [32,33]. The graphite-SbCl₅ intercalation compounds have been studied as an air-stable alternative [34]. The graphite-AsF₅ compounds have also been studied for possible use as long-wavelength monochromators, since they can be fabricated with very narrow intrinsic mosaic ($\sim 0.8^\circ$) [35].

Our efforts in studying GICs as monochromator materials were restricted to potassium-intercalated graphite. Alkali intercalation compounds were chosen due to their high reflectivity and the large body of information about them in the literature. It is expected that potassium, rubidium, and cesium intercalation compounds would perform similarly as monochromators [30]. Potassium is chosen from among these since it is the least reactive of the three and the easiest to intercalate. Also, the neutron absorption cross-section of cesium (29b) is much larger than that of potassium (2.1 b) [36], leading to greater attenuation of the transmitted and reflected beams, and increasing the potential for radiation damage of the monochromator.

Graphite forms a crystal with a layered structure. Within each layer, carbon atoms form strong covalent bonds with each other and form a 2D hexagonal lattice. Alternating layers are offset from each other so that the overall structure forms a hexagonally close-packed arrangement. The bonds between adjacent layers are extremely weak.

Intercalated graphites are formed by taking advantage of the weak bonding between layers to insert the intercalant atom or molecule between carbon layers. The introduction of the intercalant pushes the graphite layers apart and shifts the carbon planes so that the carbon atoms of adjacent layers line up. GICs are formed in discrete stages, with distinct periodicity to the arrangement of intercalant atoms within the

graphite host matrix. These stages are characterized by the stage number m , where m is the number of layers of carbon atoms between each layer of intercalant atoms.

The stage composition of an intercalated graphite sample depends upon the sample preparation method (see below). For a monochromator, only samples consisting of a single stage are desirable (to minimize the number of Bragg peaks in the diffracted beam and to maximize reflectivity of 0.89 nm neutrons). For potassium-graphite intercalation compounds, only stages 1 and 2 can be prepared with high purity; all higher stages only exist in mixtures of multiple stages [37].

2.3. Materials selection

Based upon a series of measurements, we select stage 2 potassium-intercalated highly oriented pyrolytic graphite (IHOPG) as a monochromator material. The details of our preliminary studies of mica, stage 1 IHOPG, and stage 2 IHOPG can be found in Ref. [38]. Therein, we measure the mosaic and 0.89 nm reflectivity of samples of the three potential monochromator materials. Based upon those measurements and the scattering parameters in the literature, a Monte Carlo simulation of the scattering from three hypothetical monochromators is constructed. Using this Monte Carlo simulation, estimates are made of the number of UCN which should be trapped using the magnetic trapping apparatus described in Refs. [38,39]. The simulated output spectra of the three hypothetical monochromators, relative to the NCNR NG-6 spectrum is shown in Fig. 1.

Of the three possible monochromator materials, fluorophlogopite is eliminated as its mosaic is narrower and its peak reflectivity lower than stage 2 IHOPG, which has nearly the same d -spacing. Hence, for the two almost equivalent diffraction geometries, stage 2 IHOPG offers many more reflected 0.89 nm neutrons than the fluorophlogopite.

The choice between stages 1 and 2 IHOPG relies upon more subtle considerations. Stage 1 IHOPG is measured to have a higher peak reflectivity at 0.89 nm than stage 2 IHOPG (70% vs. 50% in our preliminary measurements). Nevertheless, a com-

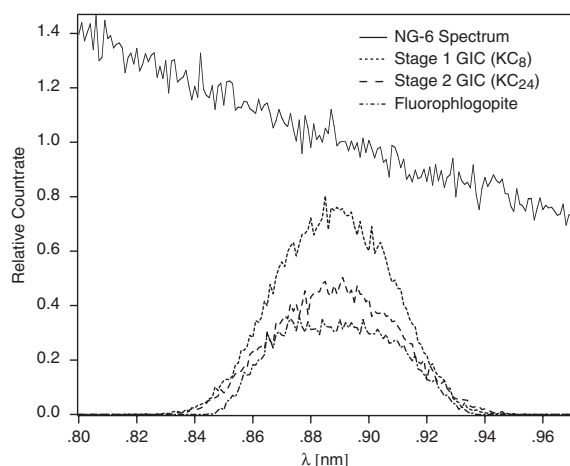


Fig. 1. The simulated neutron spectra output by three potential monochromator materials is compared to the spectrum of the NG-6 guide at the NCNR. The count rates have been scaled so that they are relative to the 0.89 nm flux of NG-6.

parable number of trapped UCN are to be expected from each monochromator due to the relative divergences of the two monochromatic beams. Since stage 2 monochromator has a smaller Bragg angle than stage 1 monochromator (30.6° , as opposed to 56.3°), the divergence of the diffracted beam will be smaller from the stage 2 monochromator. Monte Carlo simulations show that the expected lower reflectivity of stage 2 IHOPG relative to stage 1 IHOPG is made up for by its lower divergence. Stage 2 IHOPG is chosen since it has a more favorable reflected beam takeoff angle. Also, as a mosaic of a typical crystal tends to increase with deeper intercalation, stage 2 samples are easier to fabricate with desired mosaics than stage 1 samples. As will be seen below, the peak reflectivity at 0.89 nm of our final stage 2 IHOPG monochromator is higher than initially expected, making its advantage over stage 1 IHOPG substantial.

3. Fabrication of IHOPG

HOPG crystals $2\text{ cm} \times 5\text{ cm} \times 2\text{ mm}$ are intercalated using the standard “two-bulb technique” [40]. Intercalation of larger-area crystals is more

difficult as it requires longer diffusion path for intercalant atoms, producing samples with larger mosaic. In the two-bulb technique, an evacuated glass ampule with two connected, but physically distant, bulbs is prepared. The graphite to be intercalated and the intercalant material (potassium) are each located within one of the two bulbs. The ampule is then heated in a two zone furnace so that the graphite and the intercalant equilibrate at different temperatures. The rate of intercalation is determined by the potassium vapor pressure, which in turn is set by the potassium temperature, T_K . The intercalation rate affects the final mosaic of the intercalated sample. The equilibrium ratio of potassium atoms to carbon atoms in the intercalated graphite is a function of the temperature difference between the graphite and potassium, $T_G - T_K$. The phenomenon of discrete stages, which appears structurally as described above, is due to the existence of temperature plateaus in the carbon to potassium ratio.

The precise temperature differences corresponding to the plateaus for each stage depend on the detailed geometry of the intercalating ampule and the graphite sample. When preparing stage 2 potassium IHOPG it is known that the highest stage purity (minimal contamination of stages 1 and 3) is obtained close to the transition between stages 2 and 1 [37].

The temperatures of each zone of the furnace and of the intercalation cell are monitored by thermocouples and serve as a feedback to two separate heaters, one per zone. Glass wool, packed into the ends of the furnace and between the two zones, minimizes convection and provides temperature stability of about $\pm 2^\circ\text{C}$.

The optimal parameters for intercalation are determined iteratively by intercalating samples and measuring their stage purity. It is determined that samples with high stage 2 purity (no measurable stage 1 or 3 diffraction peaks) can be fabricated by heating the sample with $T_K = (206 \pm 2)^\circ\text{C}$ and $T_G - T_K = (112 \pm 3)^\circ\text{C}$ (this last constraint determines the final stage and stage purity of the intercalated crystals). Three samples were intercalated with these settings and all displayed high stage 2 purity after 4–5 days of intercalation.

4. Sample characterization

During the fabrication process, IHOPG samples are characterized by thermal neutron diffraction. Rocking curves and θ - 2θ curves are measured. Rocking curves, generally used for sample mosaics measurements, are obtained by rotating the sample while keeping the detector position fixed. θ - 2θ curves, used for measuring sample d -spacing distribution, are obtained by rotating the sample by an angle θ , while simultaneously rotating the detector around the same axis by 2θ . The use of 0.2465 nm neutrons at a thermal neutron diffractometer allows measurements to be made while the samples are still in their borosilicate glass intercalation ampules.

4.1. Stage purity

In order to determine the stage purity of the IHOPG samples, θ - 2θ curves are measured for each sample. By determining the distribution of d spacings, the presence of different IHOPG stages was determined. This diagnostic technique is used to determine the optimal temperatures for intercalation, and the necessary length of intercalation process. For example, the θ - 2θ curve for one sample is shown in Fig. 2 after two successive periods of intercalation. In this manner, high stage purity is ensured for all of the samples used in the final monochromator. Furthermore, the appropri-

ate temperatures for intercalation were determined, so that the last few samples that were intercalated reached high stage 2 purity after only a single heating period with the parameters discussed above.

4.2. Sample mosaic

The mosaic of each sample is determined using rocking curve measurements for two sample orientations: with the long axis of the sample vertical (“vertical mosaic”) or horizontal (“horizontal mosaic”). In studying the mosaics of the early samples, an unexpected characteristic is discovered. While the horizontal mosaics of the samples are simple Gaussian peaks, as expected, the vertical mosaic of almost every sample shows a double peak structure (see Fig. 3).

The double peak indicates that there are two groups of crystal planes within the sample, each of which has a comparable mosaic, but which are separated from each other by a fixed angle (about 1.5°). Both the visible appearance and the rocking curve are consistent with a distortion of the sample so that the IHOPG, viewed along the long axis, forms a “v” shape. This “v” distortion of the samples is evidently caused by the stresses of the intercalation process and was seen to some extent in each sample.

We remove the distortion by compression. A compression device (shown in Fig. 4) is con-

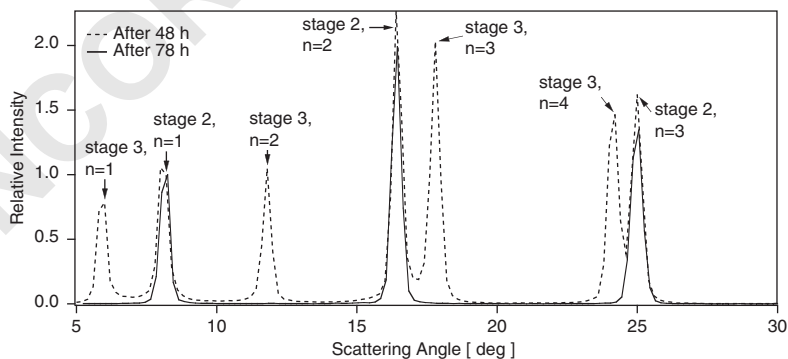


Fig. 2. θ - 2θ thermal neutron diffraction curves are shown for one of the samples after two heating periods. The sample was initially intercalated for 48 h with $T_K = 202^\circ\text{C}$ and $T_G = 323^\circ\text{C}$. The sample was then intercalated for an additional 30 h with $T_K = 205^\circ\text{C}$ and $T_G = 316^\circ\text{C}$. Following the second intercalation, stage 3 diffraction peaks are no longer evident. For both curves, the intensity has been normalized so that the relative intensity of the stage 2, $n = 1$ peak is 1.0.

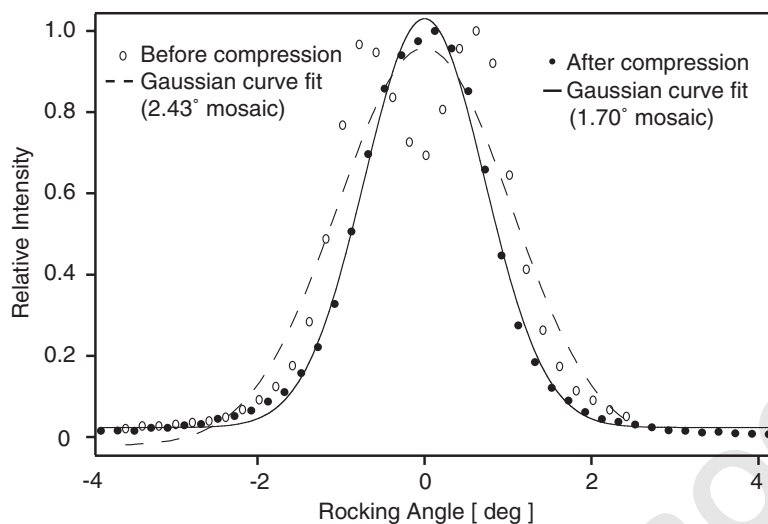


Fig. 3. The rocking curve of intercalated sample in the vertical orientation is shown before and after compression.

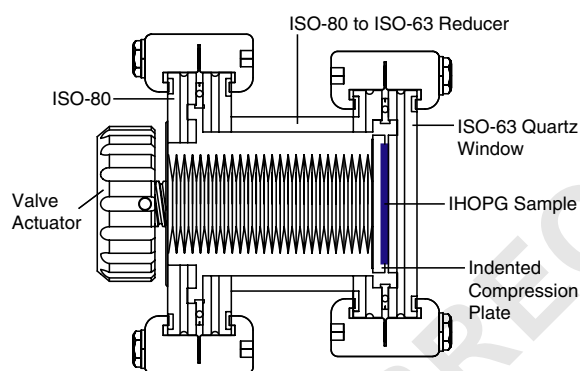


Fig. 4. The device used for compressing the samples is shown.

structed from standard vacuum components. The sample is compressed against the ISO-63 quartz window. During compression it is noted that the resistance increased discontinuously at a certain point which corresponded to a change in the area of optical contact between the sample and the window. Samples are typically left under compression for at least 24 h.

Once the compression is removed, the mosaics are remeasured. Whereas before compression two peaks are present in the rocking curve (Fig. 3), after compression only a single peak is evident. All

samples are compressed once, even if only a single peak is seen in the first rocking curve measurement. Compression makes no significant change in the mosaics of the samples which already had a single peak in their rocking curves. For some of the samples, compression reduces the separation of the two peaks in the rocking curve but does not entirely eliminate it.

5. Assembled monochromator

5.1. Sample characteristics

The nine highest-quality IHOPG samples are used in the final assembly of the monochromator. The samples are chosen for high stage 2 purity and smallest mosaics. The measured characteristics of the samples used are shown in Table 1, along with the characteristics of six samples which were not used. As can be seen, all but one of the samples used in the monochromator have minimal stage 3 contamination and only one of the samples has a double-peaked rocking curve. The samples not used all have large stage 3 contamination, multiple peaks in the vertical rocking curve, or poor reflectivity.

Sample no.	β_h (deg)	β_v (deg)	N_{peak}	R_{th}	$R_{0.89}$	$P_{3/2}$
26432	1.49	1.70	1	0.78	0.86	0.00
27524	1.24	1.91	1	0.95	0.91	0.00
27523	1.47	2.13	2	0.82	0.79	0.00
26460	1.50	1.90	1	0.80	0.85	0.01
27549	1.12	1.47	1	1.00	0.85	0.00
27537	1.31	1.43	1	0.92	0.73	0.00
27580	1.78	1.53	1	0.76	0.91	0.00
26472	1.42	1.70	1	0.88	0.90	0.00
26520	1.71	2.04	1	0.90	0.81	0.84
26519	2.27	1.94	1	0.88	0.75	0.49
27539	1.68	2.00	2	0.80		0.00
26469	1.91	2.09	2	0.66	0.86	0.06
27536	1.57	2.31	1	0.45	0.78	0.22
27533	1.80	2.31	1	0.36	0.39	3.14
27538	1.56	2.41	1	0.22		2.00

The first nine samples listed are those used in the final monochromator assembly. For each sample, the horizontal (β_h) and vertical (β_v) mosaics are shown. The number of peaks observed in the vertical rocking curve after compression is also indicated (N_{peak}). The relative thermal neutron reflectivity, R_{th} is computed as the number of counts at the Bragg peak for each sample, normalized to the most intensely reflecting sample. The measured absolute 0.89 nm reflectivity, $R_{0.89}$, is shown for the samples used in the final monochromator (see Section 6). The stage purity of each sample is indicated by $P_{3/2}$ which is the ratio of the peak heights of the stage 3, $n = 3$ and stage 2, $n = 1$ diffraction peaks on the $\theta-2\theta$ curve. The $n = 3$ peak is the most intense of all of the stage 3 peaks.

5.2. Monochromator holder

The monochromator is assembled from nine crystals tiled in a 3×3 array. The monochromator is 6 cm tall and 15 cm wide. Since the Bragg angle at 0.89 nm is 30.6° , the monochromator apparent width to the incident neutron beam is 7.6 cm. The size of the monochromator was chosen to match the $6 \text{ cm} \times 6 \text{ cm}$ area of the beam available on the NCNR NG-6 beamline.

The IHOPG samples that make up the monochromator must remain in an inert atmosphere at all times. A vacuum-tight aluminum monochromator housing, shown in Fig. 5, was thus constructed. The intercalated graphite crystals are pressed against a 3.0-mm-thick aluminum window by aluminum bars. A layer of 1 mm GoreTex GR³ gasket material is placed between the aluminum bars and the crystals to distribute the force uniformly across all three samples. The sample holder is made from aluminum to minimize

neutron activation and to maximize transmission of the reflected beam, which is greater than 99% for 0.89 nm neutrons. The monochromator is sealed in a helium atmosphere using an indium wire seal. The integrity of the indium seal is indicated by the consistency between measurements of the 0.89 nm reflectivity made more than 6 months apart.

6. Time of flight measurements

In order to measure the 0.89 nm reflectivity, a time-of-flight (TOF) spectrometer is constructed. A disc chopper with rotational frequency of 60.0 Hz is located at the exit of the NG-6 beam. The neutron beam is defined by a 3.8 mm aperture (TOF aperture) mounted on the front of the chopper and two diametrically opposite 3.8-mm-wide slits cut in a chopper disc at a radius of 15 cm. The chopper is mounted on vertical and horizontal translational stages so that it could be scanned across the beam. Neutrons are detected

³W. L. Gore & Associates, Newark, DE.

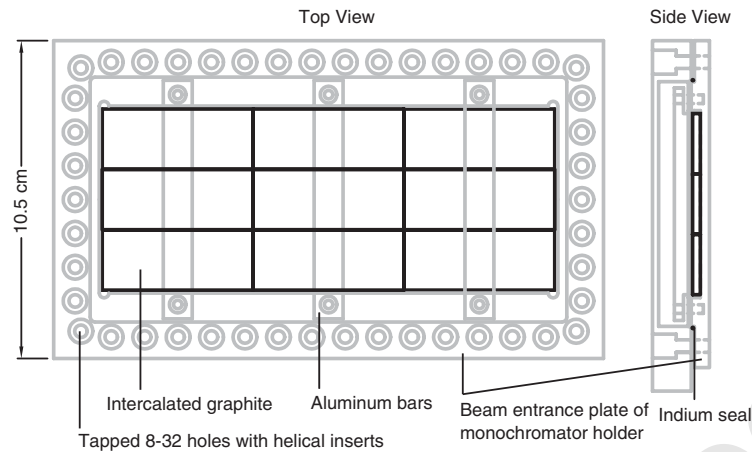


Fig. 5. Schematic view of the monochromator housing.

using 12.7 cm diameter ${}^6\text{Li}/\text{ZnS}(\text{Ag})$ scintillator⁴ coupled to a 12.7 cm bialkali Burle 8854 photomultiplier tube (PMT) biased at +1670 V. The neutron detector is located 1.9 m from the chopper. PMT pulses are counted using a multi-channel scaler which is triggered by a photosensor once per chopper rotation.

The 0.89 nm reflectivity is measured as a function of position across the face of the monochromator by scanning the chopper. Since the TOF setup has only the single defining aperture, neutrons of all wavelengths and divergences pass through the aperture and are detected. The wavelengths and divergences may vary as a function of TOF aperture position so that the measured reflectivity depends not only on the inherent properties of the monochromator crystals, but also on the distribution of neutron momenta which reach them and hence their placement in the holder.

The 0.89 nm reflectivity is determined for each aperture position by measuring the TOF spectrum with the detector in the transmission geometry. Two TOF spectra are taken, one with the monochromator aligned so that the Bragg condition is satisfied for 0.89 nm neutrons ($\theta = 30.61^\circ$), and another with the monochromator rotated off-

Bragg ($\theta = 45.61^\circ$). A typical pair of TOF spectra, in this case with the TOF aperture in line with the center of the neutron beam and the center of the monochromator, is shown in Fig. 6. Background counts are subtracted from each run by subtracting the average counts per channel over the wavelength band from 1.6 to 1.7 nm, where the neutron spectrum is observed to be flat (and should be zero). The conversion between neutron arrival time and wavelength is performed using only information within the measured spectra themselves. Three reference points are identified: the peak of the first-order Bragg reflection (determined as the peak of a Gaussian curve fit to the difference between on- and off-Bragg spectra), the peak of the second-order Bragg reflection ($\lambda/2$) and the dip in the spectrum at 0.48 nm (due to an up-beam monochromator belonging to a separate instrument).

For each pair of TOF spectra, the monochromator's reflectivity is determined over the wavelength band 0.88–0.90 nm, the wavelength band that contributes to UCN production for the deepest practical magnetic trap. The reflectivity at the center of the monochromator is $(85.4 \pm 0.6)\%$. The reflectivities measured with the beam centered on other samples are shown in Table 1. The beam is about 2 cm in diameter at the monochromator position. Hence, the measured

⁴Bicron BC-702 Thermal Neutron Scintillator. The BC-702 scintillator is based on that described in Ref. [41].

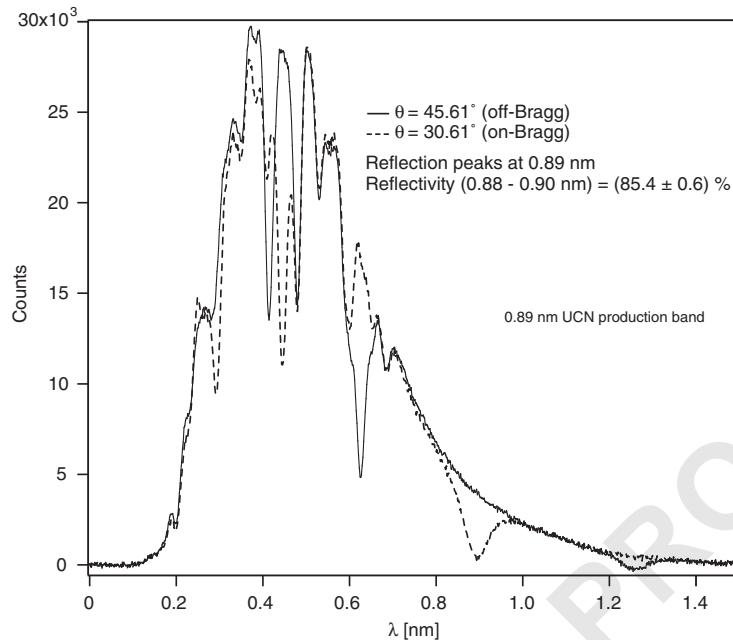


Fig. 6. TOF transmission spectrum measured with the TOF aperture in line with the center of the monochromator and the center of the neutron beam. The measurements are done with the monochromator orientations corresponding to the on ($\theta = 30.61^\circ$) and off ($\theta = 45.61^\circ$) Bragg condition for 0.89 nm neutrons.

reflectivities ascribed to each sample may depend somewhat on the reflectivities of adjacent samples.

7. Neutron wavelength filtering

In addition to reflecting 0.89 nm neutrons, the monochromator also reflects neutrons which satisfy the Bragg condition at higher order ($n \geq 2$). As can be seen in Fig. 6, the number of neutrons reflected in the $\lambda/2$ and $\lambda/3$ (with respect to $\lambda = 0.89$ nm) peaks is significant. In order to achieve the maximum possible improvement of signal-to-background ratio, it is desirable to filter out these higher-order wavelength components from the monochromatic beam.

Two techniques are used to attenuate the $\lambda/2$ diffraction peak. First, a $\lambda/2$ filter, constructed using 10-mm-thick HOPG with a mosaic of 2.2° as a 0.445 nm monochromator, is placed between the neutron guide and 0.89 nm monochromator. The broad mosaic of the filter crystal and its high reflectivity allow reduction in the $\lambda/2$ peak flux by

more than a factor of 7. TOF data comparing spectra with the $\lambda/2$ filter on and off Bragg condition is shown in Fig. 7.

The second technique, attenuating all $n \geq 2$ reflections, uses diffraction from polycrystalline materials. Such materials contain many small crystals with lattice spacings d_{cutoff} at random orientations. For a sufficiently thick crystal, any neutron with wavelength $\lambda \leq 2d_{\text{cutoff}}$ will encounter a crystal satisfying the Bragg condition and will be diffracted out of the beam. A variety of materials have been considered for use as polycrystalline neutron filters [3,4]. We restricted our tests to graphite, beryllium and polycrystalline bismuth samples and found the last of these to be the most effective.

A polycrystalline bismuth filter 10 cm diameter and 5 cm thick is prepared by compressing water quenched 99.9% pure bismuth shot with a typical grain size of 2 mm at a pressure of 200 MPa. The filter is placed in a vacuum chamber and cooled to 90 K to minimize Debye scattering. The reflection spectrum of the monochromator with the bismuth

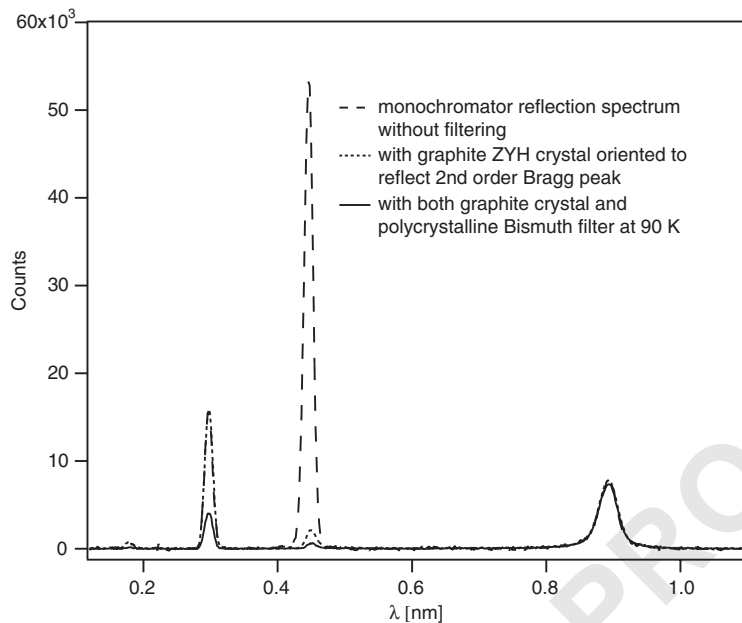


Fig. 7. TOF reflection spectrum of 0.89 nm monochromator with $\lambda/2$ filter and 5-cm-thick polycrystalline bismuth filter at 90 K. Also shown are spectra without bismuth filter and with $\lambda/2$ filter in off-Bragg condition.

filter is shown in Fig. 7. Having a Bragg cutoff of 0.65 nm [3], the filter attenuates the third-order reflection peak by 76%, while attenuation of 0.89 nm peak is only about 5%, attributed mostly to Debye scattering and absorption by impurities in the bismuth.

8. Beam characterization

The test setup of the monochromatic beam, including the placement of the primary monochromator, $\lambda/2$ filter, and existing filter cryostat (containing 5 cm of polycrystalline beryllium and 10 cm of single crystal bismuth for gamma background attenuation), is shown in Fig. 8. A variety of measurements are performed to characterize the assembled monochromator.

TOF spectra are measured with the detector in the transmission and reflection geometries and with the monochromator on and off the 0.89 nm Bragg condition. The measured TOF spectra are shown in Fig. 9. As can be seen, the number of neutrons “missing” from the dip in the transmitted

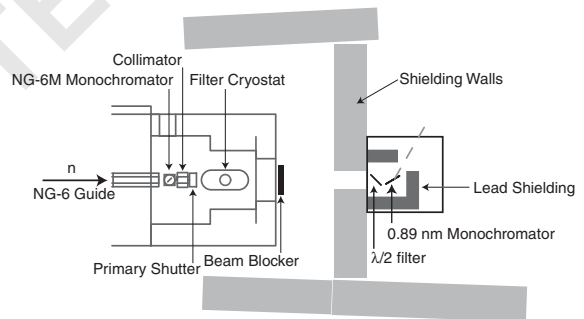


Fig. 8. Layout of the monochromatic test beam setup.

spectrum due to reflection of 0.89 nm neutrons out of the beam is equal to those “found” in the reflected neutron peak. Hence, the measured reflectivity of 85% at the center of the beam is an accurate indication of the reflectivity (absorption is negligible). The $\lambda/2$ filter can also be seen at work in the reflected spectrum. Of the neutrons in the reflected spectrum, 40% were found in the primary reflected peak, 41% in $\lambda/2$ peak and 18% in $\lambda/3$ peak. The overall fraction of the cold neutron beam reflected into the monochromatic beam is $(1.9 \pm 0.1)\%$.

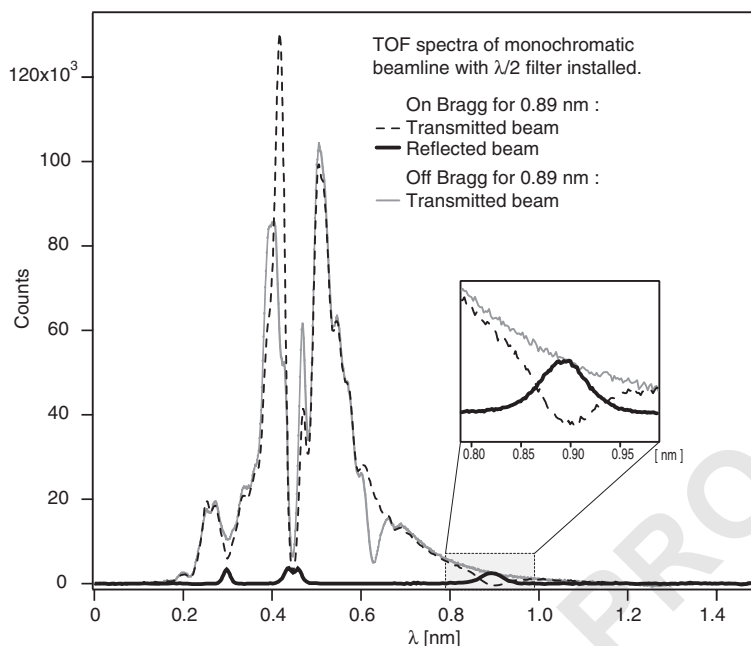


Fig. 9. TOF spectra measured with the TOF aperture in line with the center of the monochromator and the center of the neutron beam. The HOPG $\lambda/2$ filter is aligned to remove second-order reflections from the 0.89 nm monochromator. Transmission through the $\lambda/2$ filter is shown with the 0.89 nm monochromator on and off the Bragg condition. The TOF spectrum with the detector in the reflected beam is also shown.

TOF data taken 6 months later showed no major degradation of the monochromator performance. The measured reflectivity (96%) is actually slightly higher than that measured upon initial assembly and is likely due to the somewhat different geometry in this measurement. The TOF chopper was placed downstream of the monochromator, so those neutrons for which the reflectivity measurement is made are more highly collimated, which should increase the apparent reflectivity.

After confirming the satisfactory performance of the monochromator, the assembly consisting of the 0.89 nm monochromator and $\lambda/2$ filter is installed in its permanent location, upstream of the NG-6 primary shutter (Fig. 10). Shielding design in this setup does not provide access to the transmitted beam and the monochromatic beam had to be characterized using only the reflected component. First, a series of beam images is taken to adjust the monochromator tilt so that reflected neutron beam is horizontal. Then a TOF setup

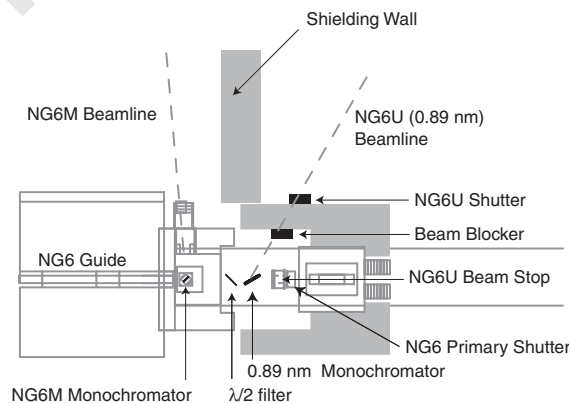


Fig. 10. Layout of the monochromatic beam setup.

similar to the one described in Section 6 is constructed, but with the chopper located downstream of the monochromator. In order to determine the wavelength calibration of the TOF spectrum, an analyzing silicon crystal with a

1 mosaic of 0.4° is mounted on a rotation stage
 2 between the monochromator and the chopper. The
 3 wavelength of the monochromatic beam can then
 4 be determined by rotating the analyzing crystal
 5 and observing changes in the TOF spectra. Indeed,
 6 if θ_1 and θ_2 are the incident angles of the neutron
 7 beam on the analyzing crystal corresponding to
 8 minimum area of $\lambda/2$ and $\lambda/3$ peaks of the
 9 primary monochromator, respectively, and $d =$
 10 0.31385 nm is the lattice spacing for 111 planes in
 11 silicon crystal, then

$$13 \quad 2d \sin \theta_1 = \frac{\lambda}{2},$$

$$15 \quad 2d \sin \theta_2 = \frac{\lambda}{3}$$

17 and λ can be calculated as

$$19 \quad \lambda = 12d \frac{\sin(\theta_1 - \theta_2)}{\sqrt{13 - 12 \cos(\theta_1 - \theta_2)}}.$$

21 A second method to calculate λ is to rotate the
 22 analyzing crystal by $2\theta_{\text{Bragg}}$ between two Bragg
 23 positions in parallel and anti-parallel orientations
 24 (with respect to the monochromator). Then $\lambda =$
 25 $2nd \sin \theta_{\text{Bragg}}$ for the analyzing crystal in the Bragg
 26 orientation for neutrons with wavelength λ/n . The
 27 value of λ obtained by this method is consistent
 28 with the result from the first method.

29 By adjusting the rotation angle of the mono-
 30 chromator and measuring the wavelength of the
 31 reflected beam iteratively, the first-order reflection
 32 peak is tuned to $\lambda = (0.893 \pm 0.002)$ nm.

35 8.1. Flux measurements

37 The neutron beam flux is measured in several
 38 positions using a calibrated fission chamber with a
 39 1-cm-diameter active region, containing a 503 ng
 40 ^{235}U deposit. The capture flux of the NG-6
 41 polychromatic beam before the NCNR neutron
 42 cold source upgrade⁵ (with 5 cm of polycrystalline
 43 beryllium and 10 cm of single crystal bismuth in
 44 the filter cryostat, see above) was measured to be
 45 $(7.6 \pm 1.9) \times 10^8$ n cm⁻² s⁻¹ at the exit of the NG-6

47 ⁵The upgrade of the NCNR liquid hydrogen neutron
 moderator yielded an increase of the neutron flux at 0.89 nm
 by a factor of 1.8.

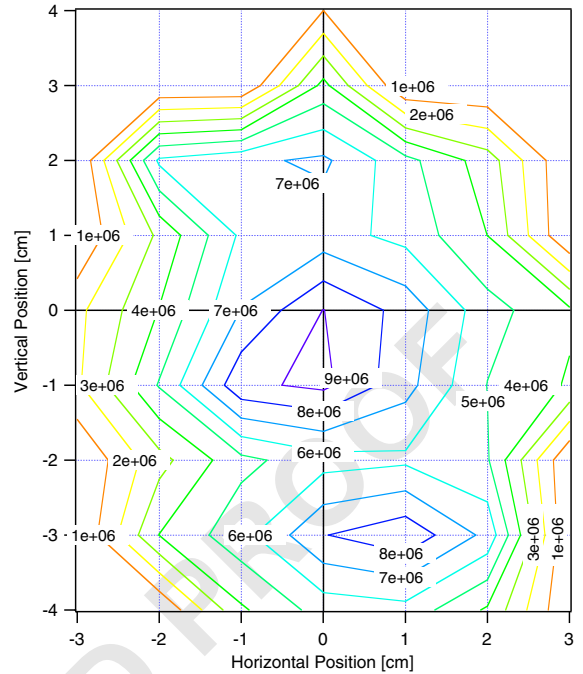


Fig. 11. The monochromatic beam flux ($\text{cm}^{-2} \text{s}^{-1}$) is measured using a fission chamber with a 1-cm-diameter active area. The measured flux is shown as a function of the position of the center of the aperture, relative to the center of the 300 K end flange of the neutron trapping apparatus.

shielding. The dominant error contribution is from uncertainty in the position of the fission chamber.

The capture flux of the monochromatic beam (Fig. 8) is measured as a function of position using the same fission chamber. The fission chamber, placed 89 cm downstream from the monochromator, is scanned in two directions perpendicular to the monochromatic beam. The measured flux as a function of position is shown in Fig. 11. As it was mentioned in Section 8, about 40% of the reflected neutrons are in the primary reflection band at 0.89 nm.

From the measured polychromatic beam flux of 7.6×10^8 n cm⁻² s⁻¹ and the measured total monochromator reflectivity of 1.9%, one can calculate the expected flux of the monochromatic beam to be 1.4×10^7 n cm⁻² s⁻¹. Correcting for the divergence of the neutron beam over the 2.21 m flight path between the positions where the

polychromatic and monochromatic flux are measured, the expected monochromatic flux decreases⁶ to $7 \times 10^6 \text{ n cm}^{-2} \text{ s}^{-1}$. The consistency of the expected and measured monochromatic fluxes indicate that the TOF data and the flux measurements are in agreement. An estimated $1.3 \times 10^6 \text{ n cm}^{-2} \text{ s}^{-1}$ of the total reflected flux is in the primary reflection peak at 0.89 nm (see Fig. 9).

The measurements of the monochromatic beam flux were repeated after the neutron cold source upgrade and installation of the monochromator in a permanent location. The flux at 0.89 nm, measured in the center of the monochromatic beam 130 cm downstream from the monochromator, is found to be $3.0 \times 10^6 \text{ n cm}^{-2} \text{ s}^{-1}$, consistent with expectations.

9. Conclusions

A 0.89 nm monochromator is constructed using stage 2 potassium-intercalated graphite. The monochromator, tiled from nine pieces, has a total size of 6 cm × 15 cm. The individual monochromator pieces have high stage purity and mosaics varying from 1° to 2°. The monochromator reflects more than 80% of the incident 0.89 nm neutrons, while reflecting less than 2% of the total cold neutron beam. The signal to neutron-induced-background ratio in the magnetic trapping experiment should be improved by a factor of 40 through use of the monochromator.

Acknowledgements

We thank J.M. Rowe, D.M. Gilliam, D.L. Jacobson, S. Werner, J. Lynn, T. Haus, T. Udovic, S.K. Lamoreaux, J.S. Butterworth., N. Clarkson,

and J. Anderson. We especially thank D. Neumann for stimulating discussions and suggestions throughout. Neutron facilities used in this work were provided by the NIST Center for Neutron Research and the Hahn Meitner Institut. This work was supported in part by the National Science Foundation under Grant No. PHY-0099400.

References

- [1] V. Wagner, H. Friedrich, P. Wille, *Physica B* 938 (1992) 180. 61
- [2] B. Hammouda, *Nucl. Instrum. Methods Phys. Res. A* 321 (1992) 275. 63
- [3] P.A. Egelstaff, R.S. Pease, *J. Sci. Instrum.* 31 (1954) 207. 65
- [4] A.K. Freund, *Nucl. Instrum. Methods Phys. Res.* 213 (1983) 495. 65
- [5] J.M. Doyle, S.K. Lamoreaux, *Europhys. Lett.* 26 (1994) 253. 67
- [6] P.R. Huffman, C.R. Brome, J.S. Butterworth, K.J. Coakley, M.S. Dewey, S.N. Dzhosyuk, R. Golub, G.L. Greene, K. Habicht, S.K. Lamoreaux, C.E.H. Mattoni, D.N. McKinsey, F.E. Wietfeldt, J.M. Doyle, *Nature* 403 (2000) 62. 69
- [7] R. Golub, D. Richardson, S.K. Lamoreaux, *Ultra-Cold Neutrons*, Adam Hilger, Bristol, 1991. 73
- [8] D. Dubbers, *Prog. Part. Nucl. Phys.* 26 (1991) 173. 75
- [9] R. Golub, *Rev. Mod. Phys.* 68 (1996) 329. 75
- [10] R. Golub, J.M. Pendlebury, *Phys. Lett.* 53A (1975) 133. 77
- [11] R. Golub, J.M. Pendlebury, *Phys. Lett.* 62A (1977) 337. 77
- [12] W.G. Stirling, Precision measurement of the phonon dispersion relation in superfluid ⁴He (1983) 109. 79
- [13] H. Yoshiki, K. Sakai, M. Ogura, T. Kawai, Y. Masuda, T. Nakajima, T. Takayama, S. Tanaka, A. Yamaguchi, *Phys. Rev. Lett.* 68 (1992) 1323. 81
- [14] R. Golub, S.K. Lamoreaux, *Phys. Rep.* 237 (1994) 1. 81
- [15] E. Korobkina, R. Golub, B.W. Wehring, A.R. Young, *Phys. Lett. A* 301 (2002) 462. 83
- [16] W.H. Zachariasen, *Theory of X-Ray Diffraction in Crystals*, Wiley, New York, 1945. 85
- [17] C.G. Darwin, *Philos. Mag.* 27 (1914) 315. 85
- [18] C.G. Darwin, *Philos. Mag.* 43 (1922) 800. 87
- [19] M.L. Crow, *Physica B* 241–243 (1998) 110. 87
- [20] A.N. Goland, J.J.H. Sondericker, J.J. Antal, *Rev. Sci. Instrum.* 30 (1959) 269. 89
- [21] T.W. Dombeck, J.W. Lynn, S.A. Werner, T. Brun, J. Carpenter, V. Krohn, R. Ringo, *Nucl. Instrum. Methods Phys. Res.* 165 (1979) 139. 91
- [22] T.O. Brun, J.M. Carpenter, V.E. Krohn, G.R. Ringo, J.W. Cronin, T.W. Dombeck, J.W. Lynn, S.A. Werner, *Phys. Lett. A* 75 (1980) 223. 93
- [23] J.W. Lynn, W.A. Miller, T.W. Dombeck, G.R. Ringo, V.E. Krohn, M.S. Freedman, *Physica B* 120 (1983) 114. 95

⁶The divergence can be roughly corrected by considering the polychromatic beam to have 6 cm diameter at the exit of the NG-6 shielding. Given the expected beam divergence of 1°, the 0.5 cm radius aperture of the fission chamber can accept neutrons from a 4.4 cm radius neutron beam 221 cm away. The effective reduction of the flux due to divergence is then the ratio of the actual beam to the potentially accepted beam: $(\frac{3}{4})^2 \approx 0.5$.

- 1 [24] K.T. Forstner, L. Passel, C.F. Majkrzak, Synthetic mica
monochromator project, personal communication.
- 3 [25] F.M. Zelenyuk, K.N. Zaitsev, A.V. Timakov, I.N. Anikin,
S.I. Matveev, V.E. Zhitarev, S.V. Stepanov, *Instrum. Exp.*
5 *Tech.* 16 (1973) 399.
- 7 [26] K. Inoue, T. Kanaya, Y. Kiyonagi, S. Ikeda, K. Shibata,
H. Iwasa, T. Kamiyama, N. Watanabe, Y. Izumi, *Nucl.*
9 *Instrum. Methods Phys. Res. A* 309 (1991) 294.
- [27] C. Shafthäutl, *J. Prakt. Chem.* 21 (1841) 129.
- [28] H. Zabel, S.A. Solin (Eds.), *Graphite Intercalation*
11 *Compounds I: Structure and Dynamics*, Springer Series
in Materials Science, Vol. 14, Springer, Berlin, 1990.
- [29] H. Zabel, S.A. Solin (Eds.), *Graphite Intercalation*
13 *Compounds II: Transport and Electronic Properties*,
Springer Series in Materials Science, Vol. 18, Springer,
Berlin, 1992.
- [30] A. Boeuf, A. Freund, R. Caciuffo, A. Hamwi, P. Touzain,
15 *Synth. Met.* 8 (1983) 307.
- [31] Db21, web page, <http://www.ill.fr/yellowbook/db21/>.
- 17 [32] N. Akuzawa, T. Fukisawa, T. Amamiya, Y. Takahashi,
Synth. Met. 7 (1983) 57.
- [33] N. Akuzawa, T. Seino, A. Yugeta, T. Amemiya, Y.
19 Takahashi, *Carbon* 25 (1987) 691.
- [34] P.C. Eklund, H.G. Smith, *J. Appl. Crystallogr.* 17 (1984)
21 400.
- [35] J.E. Fischer, J.W. Milliken, A. Magerl, H.J. Kim, A.W.
23 Moore, *Nucl. Instrum. Methods Phys. Res. A* 300 (1991)
207.
- [36] J.R. Parrington, H.D. Knox, S.L. Breneman, E.M. Baum,
25 F. Feiner, *Nuclides and Isotopes: Chart of the Nuclides*,
General Electric Co. and KAPL, Inc., 1996.
- [37] M.E. Misenheimer, H. Zabel, *Phys. Rev. Lett.* 54 (1985)
27 2521.
- [38] C.E.H. Mattoni, Magnetic trapping of ultracold neutrons
29 produced from a monochromatic cold neutron beam,
Ph.D. Thesis, Harvard University, 2002.
- [39] D.N. McKinsey, Detecting magnetically trapped neutrons:
31 liquid helium as a scintillator, Ph.D. Thesis, Harvard
University, 2002.
- [40] A. Hérold, *Bull. Soc. Chim. Fr.* 187 (1954) 999.
- [41] R. Stedman, *Rev. Sci. Instrum.* 31 (1956) 1156. 35